Structure of Poly(vinylidene difluoride) Solutions in Acetone

Dominique Sarazin,*,† Claude Picot,† and Stanislav Patlazhan*,‡

Institut Charles Sadron, CNRS, Strasbourg, 4 rue Boussingault, F-67000 Strasbourg, France, and N. N. Semenov Institute of Chemical Physics of Russian Academy of Science, 4 Kosygin Street, 119991 Moscow, Russia

Received April 4, 2005; Revised Manuscript Received December 1, 2005

ABSTRACT: Light scattering structural studies of poly(vinylidene difluoride) (PVDF) solutions in acetone have been carried out. They reveal the pronounced peaks in the wide-angle scattering profiles at polymer weight concentrations from 0.5% to 20%. The angular positions of the peaks are found to depend substantially on polymer concentration: the greater is the concentration, the larger the scattering angle corresponding to the peak maximum. These observations point to the fact that ordered polymer microstructures arise in the solutions investigated. A theoretical analysis of the experimental data suggests that the structure of PVDF−acetone solutions can be represented by a set of randomly oriented domains consisting of ordered bunches of the fiberlike constituents. Correlations of the temperature and concentration behavior of the light scattering peaks with the dimension characteristics of the structural domains are analyzed.

1. Introduction

The poly(vinylidene difluoride) is widely utilized in the fabrication of porous, ultrafiltration membranes used in numerous applications such as water treatment, medical purification, food concentration, dairy filtration, ion exchange, and gas separation. The membranes are usually prepared by exposure of homogeneous polymer solutions to an excess of a precipitator and their resulting structural characteristics—pore size distribution, texture, etc.—are rather sensible to the origin of phase separation as well as casting conditions.[1−6] The fibrillar organization is a common attribute of the PVDF membranes.[7,8] This type of structure has been observed in films cast from the PVDF−acetone solutions with polymer concentrations ranging between 4 and 10 wt %.[9] Furthermore, the wide-angle X-ray scattering from the membranes reveals periodic fluctuations, which were interpreted as an alternation of the crystalline and the amorphous regions.[10−11]

These observations indicate that morphology of PVDF membrane is defined by a set of successive self-organization processes. One could expect a priory that these structural formations may arise in the solute state. Nevertheless, current studies disregarded this point while it may be important in development of membrane morphology. At the same time, preliminary investigation of light scattering from PVDF solutions in acetone showed the presence of single peaks within the scattering profiles.[12] This effect prompts occurrence of organized microstructures prior to the film casting and stimulates their investigation. Under the more general aspects, this research might illuminate peculiarities of hierarchical self-organization in polymer solutions, in particular, of perfluorinated polymers.

In the present work, the systematic structural studies of PVDF−acetone solutions are carried out. The main attention is focused on revealing characteristics of solution morphology by means of structural model providing the same optical effects.

The paper is organized as follows. The materials data and the experimental technique are presented in the next section. The experimental results including wide- and small-angle light scattering data for PVDF−acetone solutions at different concentrations and temperatures are reviewed in section 3 along with an electron microscope observation of the cast films. A theoretical study of the scattering effects, in terms of a representative structural model, is developed in section 4. The comparative analysis of experimental and theoretical results is detailed in section 5.

* To whom correspondence should be addressed. E-mail: (S.P.) sapat@polymer.chph.ras.ru; (D.S.) sarazin@ics.u-strasbg.fr.

† Institut Charles Sadron.

‡ N. N. Semenov Institute of Chemical Physics.

2. Materials and Methods

2.1. Materials. Elf Atochem (ATOFINA) has supplied the pellets of poly(vinylidene difluoride) labeled as KYNAR 740. The PVDF chemical composition consists of linear sequence of monomers $-CH_2-CF_2-$. This polymer was shown to contain alternation defects of CH_2 and CF_2 groups that may lead to aggregation of PVDF chains resulting in creation of physical microgels.[15,16] In our experiments, KYNAR 740 has been purified by precipitation in methanol or heptane from the hot acetone or isophorone solutions. The dust particles were removed from the pure solvent with Dynaguard 0.45 μm filters of Microgon Inc.

Examination of molecular characteristics of KYNAR 740 was made at room temperature in dilute solutions of acetone and *N*,*N*-dimethylformamide (DMF) by means of static (SLS) and dynamic (DLS) light scattering. The second virial coefficients of PVDF measured by SLS are about $A_2 = -5 \times 10^{-5}$ mL·mol·g^{-2} for acetone and $A_2 = 1.7 \times 10^{-7}$ mL·mol·g^{-2} for DMF, respectively. These values indicate that acetone is a poor solvent while DMF is a good solvent, which are in close proximity to the theta point. At the same time SLS was unable to provide accurate dimensions of PVDF in the dilute solutions because of violation the Guinier range condition near the smallest scattering angle available. These characteristics were measured by the dynamic light scattering. The analysis of the obtained autocorrelation function $g^{(2)}(q,t)$ of the light scattering intensity (see below) revealed sharp single-peaked distributions of relaxation times. This is relevant to presence of the well-defined monodisperse inclusions in both of solvents. Their hydrodynamic radii were found to equal to $R_H = 270$ nm in acetone and $R_H = 330$ nm in DMF, respectively. These dimensions indicate that PVDF units are more compact in acetone than in DMF, which correlates with the obtained second virial coefficients.

The obtained characteristics are coherent with SLS data extracted from the Guinier plot. The average gyration radius of PVDF formations in dilute acetone solutions is about $R_G = 228$ nm. The ratio of this size to the corresponding hydrodynamic radius is about

10.1021/ma050697e CCC: $33.50
Published on Web 01/05/2006

$\rho = R_G/R_H \cong 0.84$, which is rather close to the hard sphere value of 0.78.

2.2. Static Light Scattering. The wide- and the small-angle static light scattering experiments were carried out. The wide-angle scattering intensity was measured by the in-house apparatus[13] equipped with (i) a red He−Ne laser of wavelength $\lambda_0 = 632.8$ nm in a vacuum, (ii) a discrete-angle goniometer acting within the range from 20° to 155°, (iii) a Hamamatzu type photomultiplier as detector, (iv) a photocounting device, and (v) a toluene matching bath. The vertical polarization of the incident beam with respect to the scattering plane has been used. The analyzer, arranged between the measuring cell and the photomultiplier, could assume both the vertical and the horizontal orientations. The first position allows measurement of the isotropic V_V scattering while the second was applied in the study of the depolarized H_V scattering.[14] The excess of light scattering intensity $I(q) = I_{solution} - I_{solvent}$ was measured as a function of scattering vector $q = (4\pi n/\lambda_0)\sin\theta/2$ with an accuracy of 1% (θ is the scattering angle). The values of scattering intensity $I(q)$ were obtained through the calibration with a benzene standard. The acetone refractive index and the average refractive index increment of PVDF relative to acetone are equal to $n = 1.359$ and $dn/dc = 0.064$ mL/g, respectively.

The small-angle light scattering patterns were recorded using an Ikegami ICD42E analogical camera. The obtained H_V scattering images were analyzed and digitalized through the meteor-Matrox card implemented by the in-house software.

2.3. Dynamic light scattering measurements were made on the ALV/DLS/SLS-5020F (ALV-Laser Vertriebsgesellshaft mbH, Langen, Germany) consisting (i) a He−Ne laser ($\lambda_0 = 632.8$ nm), (ii) ALV/CGS-8 goniometer system working in the range from 22° to 145°, and (iii) ALV-5000 autocorrelator. The normalized autocorrelation function[18] $g^{(2)}(q,t) = 1 + [\int P(\tau)\exp(-t/\tau)\,d\tau]^2$ was analyzed by means of the CONTIN program[19] integrated into ALV software ($P(\tau)$ is the distribution function of relaxation time τ). The apparent hydrodynamic radii R_H of polymer formations in the dilute solutions were estimated from the Stokes−Einstein relationship $\tau(q) = 6\pi\eta_s R_H/q^2 k_B T$ under assumption that scattering elements are of spherical shapes.

2.4. Electronic Microscopy. The morphologies of the cast PVDF films were visualized using a Philips CM12 transmission electronic microscope operating at 120 kV. The microscope was used in the image mode with the refracted beam focused on the screen. The dark patches of the image reveal the crystalline mats. The thickness of the samples used was less than 1 μm to obtain better images. To achieve this limit, the water casting was carried out from the dilute solutions, followed by the slow drying of the films deposited on a carbon grid. The film morphology was observed directly on a screen without the metal shadowing.

3. Experimental Results

3.1. Peculiarities of Static Light Scattering. PVDF−acetone solutions are visually opalescent in the range of polymer concentration c_p from 1% to 10%. A further increase in PVDF concentration until $c_p \cong 18\%$ leads to a slight turbidity. This upper limit corresponds to the point of physical gelation at the room temperature $T = 25$ °C. Above the threshold corresponding to $c_p \sim 30\%$, the crystallites grow thus elevating sample turbidity.

Measurement of the wide-angle light scattering from the solutions reveals distinct peaks at polymer concentrations from 0.5% to 20%. The peaks are found to appear within the range of the scattering vector from $q \cong 4 \times 10^{-3}$ to 1.8×10^{-2} nm^{-1}. It is notable that the observed optical effect takes place at polymer concentrations well below the referred characteristic points.

Three examples of the V_V scattering profiles corresponding to $c_p = 2\%$, 5%, and 10 wt % measured at $T = 42$ °C are illustrated in Figure 1. The scattering intensity is expressed here in terms of reduced value $I(q)/(Kc)$ where $K = K_{benzene}(dn/dc)^2$ is the optical contrast calibrated with benzene standard. The positions of the scattering peaks are seen to depend on polymer concentration: the higher is the polymer concentration, the larger the scattering vector q^*, corresponding to the maximum intensity. The amplitude and the shape of the peaks are correlated with PVDF concentration as well. In particular, an increase in polymer concentration results in a decrease of the peak. The shapes of the signals are seen to be rather regular below the gelation point. They become irregular at concentrations exceeding $c_p \cong 18\%$. This fact is demonstrated in the inset of Figure 1 giving the scattering profile of the 20% solution.

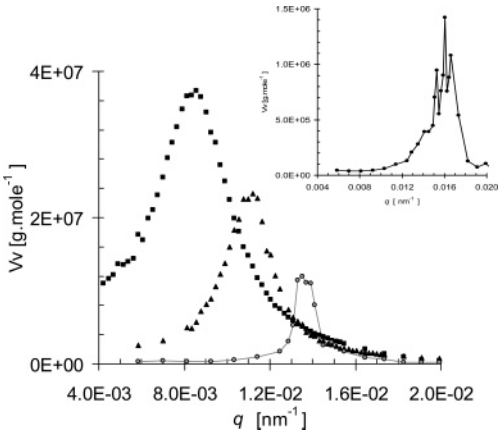

Figure 1. Normalized V_V scattering intensity profiles of PVDF−acetone solutions measured at $T = 42$ °C for different polymer concentrations: (■) 2%; (▲) 5%; (●) 10%. The inset corresponds to the 20% PVDF−acetone solution.

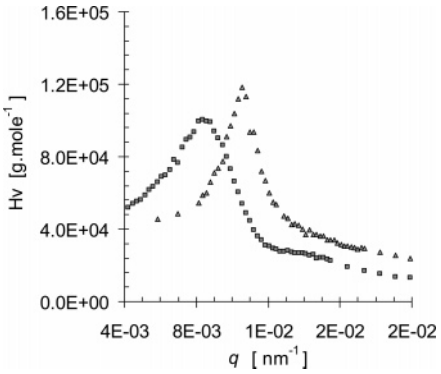

Figure 2. Normalized H_V scattering intensity profiles of PVDF−acetone solutions measured at $T = 42$ °C for different polymer concentrations: (■) 2%; (▲) 5%.

The depolarized H_V scattering is shown in Figure 2 for the 2% and 5% PVDF−acetone solutions. This plot reveals surges of the scattering intensity as it was demonstrated before. The positions of the H_V scattering peaks coincide with those of the V_V peaks at the same polymer concentrations. Thus, the increase in PVDF content leads to a shift of H_V peaks toward larger scattering vectors. Nevertheless, contrary to the V_V scattering, the magnitudes of the H_V peaks increase with the increasing of polymer concentration. The existence of the depolarized scattering reveals the optical anisotropy of scattering units.

The dependence of the V_V and H_V scattering profiles on temperature is displayed in Figures 3 and 4 at the concentration $c_p = 2\%$. The temperatures studied are in the range 25 to 91°C. The upper limit exceeds the boiling point of acetone. To make measurements under these conditions, a special pressure cell equipped with a window for the scattered light was designed. Figures 3 and 4 indicate that temperature has no influence on the peak position. However, raising the temperature results in

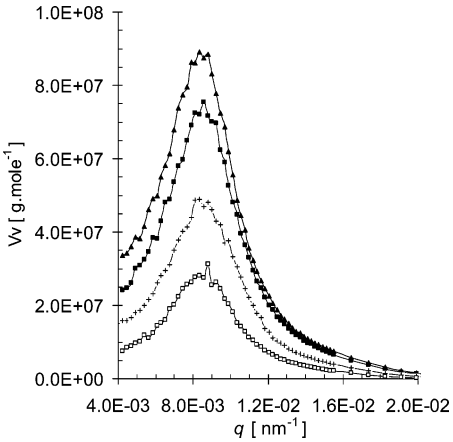

Figure 3. Temperature dependence of normalized V_V scattering profiles of 2% PVDF−acetone solutions: (□) 25 °C; (+) 50 °C; (■) 76 °C; (▲) 91 °C.

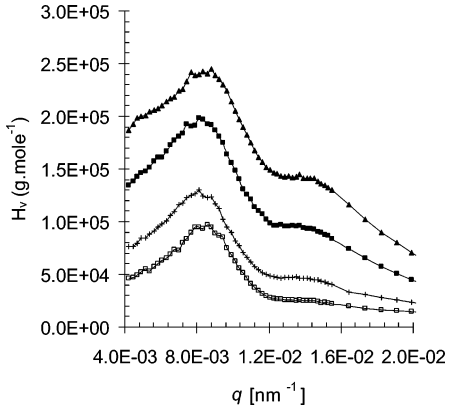

Figure 4. Temperature dependence of the normalized H_V scattering profiles of 2% PVDF−acetone solutions: (□) 25 °C; (+) 50 °C; (■) 76 °C; (▲) 91 °C.

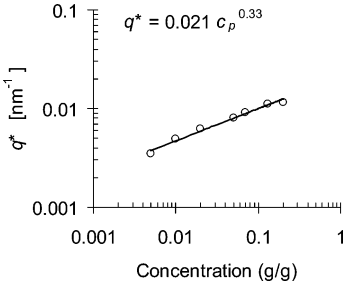

Figure 5. Dependence of maximum positions q^* of V_V scattering peaks on PVDF concentration. The power-like dependence $q^* \sim c_p^{0.33}$ indicates the 3D dense packing of the ordered domains in the solutions.

an increase in the peak height both for isotropic and depolarized light scattering. The observed behavior of V_V and H_V scattering profiles indicates that dimensions of scattering elements rather than their optical anisotropy control the peak amplitude.

It is worth noting that value q^* of scattering vector corresponding to the peak maximum is a power function of polymer concentration, $q^* \sim c_p^{0.33}$. This is shown in Figure 5 demonstrating linear dependence of $\log(q^*)$ on $\log(c_p)$ in a broad range of polymer concentrations. This sort of dependence implies that structure of PVDF−acetone solutions may be represented as a close packing of ordered scattering domains.

3.2. Spherulite Signature. The spherulite structure has been found in 20% PVDF gels immersed in a poor binary solvent (DMF + octanol) by means of DSC and small-angle light scattering.[5] However, at lower polymer concentrations these

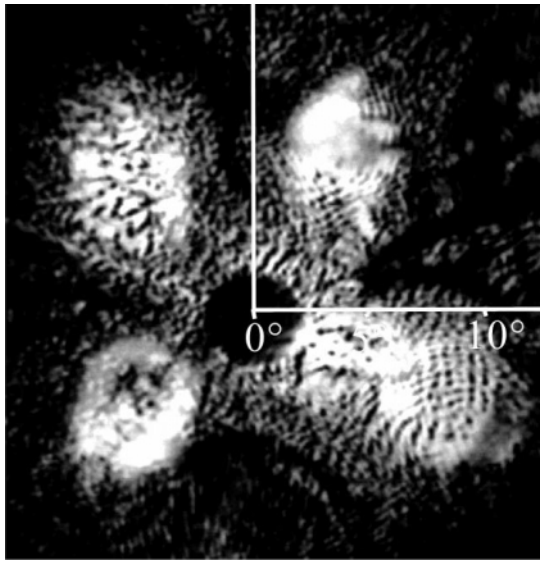

Figure 6. CCD image of the anisotropic H_V light scattering by 10% PVDF−acetone solution. This picture indicates an occurrence of fiberlike structure with random orientation.

measurements become difficult because of the low level of the depolarized scattering intensity. Nevertheless, we were able to obtain H_V scattering patterns with a red He−Ne laser and a CCD camera as a detector. Figure 6 shows an example of the pattern corresponding to the 10% PVDF−acetone solution at room temperature. A low level of scattering intensity is caused by either small density or low optical anisotropy of the scattering elements. The fuzzy four-leaf clover image indicating preexistence of spherulites is observed. However, in contrast to the perfect spherulite light scattering pattern, the nonzero intensity could be observed near the center of this picture. It may be understood as an interference of light scattered both from spherulite-like formations and randomly orientated domains of microfibers.

An average size of these elements may be roughly estimated using the familiar expression $R_s = 4/q_{max}$ for spherulites[20] where q_{max} is the average magnitude of the scattering vector corresponding to maximum intensity at the scattering pattern (see Figure 6). Taking into account that the average scattering angle at these points is $\theta_{max} \cong 5°$, the average size of the scattering elements is $R_s \cong 3.5\ \mu$m.

3.3. Structure of Cast PVDF Films. Figure 7 gives the electron microscopy image of the film cast from a 5% PVDF−acetone solution on a water surface. It reveals a two-phase structure, which is represented by thin fibrous ligaments containing inclusions of a brighter contrast. The average size of these inclusions is of the same order as hydrodynamic length of PVDF formations measured by the dynamic light scattering (see section 2.3). Below we will assume that the weblike fibrous formations are the basic constituent of structure of PVDF−acetone solutions.

4. Theoretical Analysis

4.1. Structural Model. The foregoing experiments suggest the development of ordered microstructures in PVDF−acetone solutions at polymer concentrations in the range from 0.5% to 20%. Specifically, the small angle light scattering suggests an existence of the large-scale spherulite-like domains, while the wide-angle scattering peaks hint at a spatial ordering within the formations. To reveal structural peculiarities of the solutions, an appropriate model providing the same optical effects should be constructed.

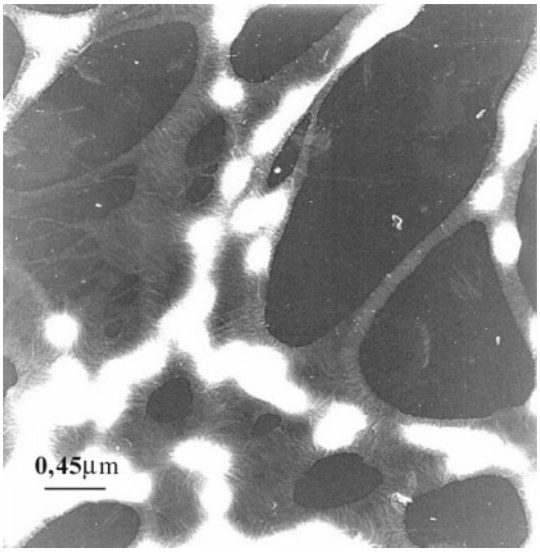

Figure 7. Electronic microscope image of a 5% PVDF−acetone solution poured on a water surface. The magnification is 22 000×.

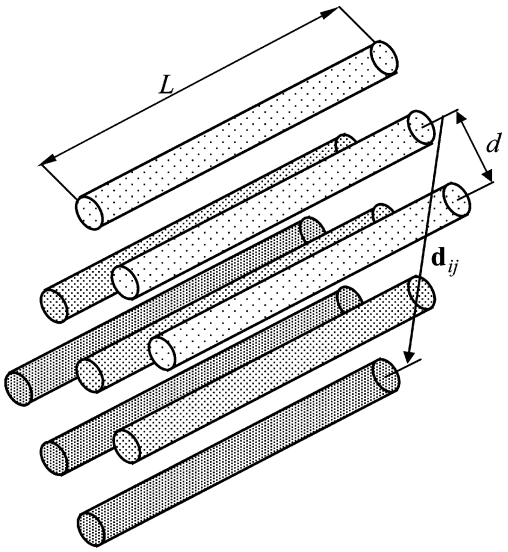

Figure 8. Structural model of the ordered fibrous domain.

Toward this end, we suppose that the structure of PVDF−acetone solutions possesses some quality inherent to the dry films cast from the solutions. Particularly, we assume that the structure of the solution is represented by a set of randomly oriented domains consisting of ordered fiberlike formations. The thin ligaments in Figure 7 could presumably represent some of these microfibers. The structure may be formed due to the self-association of PVDF chains caused by the alternation defects of CH_2 and CF_2 groups mentioned in section 2.1. An increase in temperature would result in disintegration of physical bonds between the neighboring macromolecules followed by shrinkage of the microfibers, thus reducing their lengths. In turn, an increase in polymer concentration would lead to a more dense structure involving a reduction of the average distance between the microfibers.

The schematic representation of this kind of domains is given in Figure 8, illustrated as a bunch of N_r ordered rods. This model is supposed to be a representative structural element of PVDF−acetone solutions. For the sake of simplicity, the microfibers constituting the domain are taken of the same average length L and radius R; their centers are assumed to form a 2D hexagonal lattice in the domain cross-section with average distance $\bar{d}$ between the nearest rods.

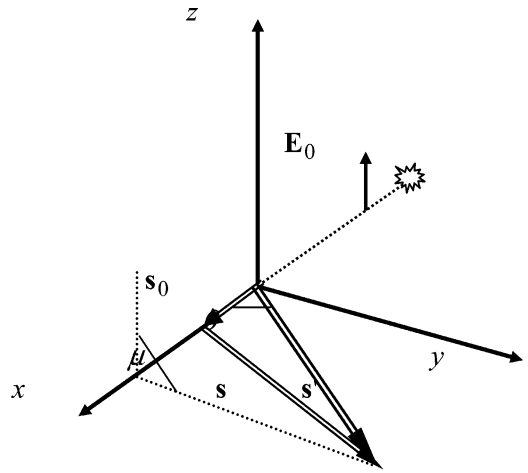

Figure 9. Scheme of wide-angle light scattering experiment.

Running a few steps forward, we note that neither spherical nor disklike formations arranged in any periodical 3D structure could provide similar scattering peaks as were observed in our experiments.

4.2. Light Scattering from Parallel Rod Domains. The light scattering from a single rod has been treated theoretically a long time ago. An isotropic cylinder or anisotropic infinitely thin rods were considered in most of the papers.[21] The comprehensive solutions for the optically anisotropic cylinder of arbitrary sizes and orientation were obtained by van Aartsen.[22] The results as applied to the wide-angle scattering are presented in Appendix I.

The measurements were performed in a horizontal plane including the incident beam and the wave vector $\mathbf{k}'$ of the scattering light. The wave vector $\boldsymbol{k}_0$ and the polarization of the ray are considered to orient respectively along the x- and z-axes of the laboratory coordinate frame as illustrated in Figure 9. Thus, the scattering vector $\mathbf{q} = \boldsymbol{k}_0 - \mathbf{k}' = q\mathbf{s}$ is located in the (x,y)-plane keeping the azimuthal angle $\mu = 90°$.

In line with general theory,[23] the scattering intensity from a set of N_r parallel rods may be represented as

$$I_{\text{domain}}(q,L,R,\alpha,\Omega,\phi,d,N_r) = I_1(q,L,R,\alpha,\Omega)\{N_r + \sum_{m\neq n}^{N_r}\sum \exp(i\mathbf{q}\mathbf{d}_{mn})\} \quad (1)$$

where $I_1(q,L,R,\alpha,\Omega)$ is the scattering intensity from a single rod (see Appendix I); α and Ω are the polar and azimuthal angles with respect to the reference system (x',y',z') which is associated with the vector $\mathbf{q}$ (see Figure 14); $\mathbf{d}_{mn}$ is the distance between the mth and nth rods. The inner product $\mathbf{q}\mathbf{d}_{mn}$ equals to

$$\mathbf{q}\mathbf{d}_{mn} = qd_{mn}\cos(\phi + \psi_{mn})\sin\alpha \quad (2)$$

The angles ψ_{mn} and ϕ characterize orientation of vector $\mathbf{d}_{mn}$ and the hexagonal lattice relative to the rod's coordinate system (x'',y'',z'').

The relative scattering intensity from randomly orientated domains corresponds to the averaging of eq 1 over the angles α, Ω, and ϕ:

$$\bar{I}_{\text{domain}}(q,L,R,d,N_r) = \frac{1}{(2\pi)^2}\int_0^{\pi}\int_0^{2\pi}\int_0^{\pi} I_{\text{domain}}(q,L,R,\alpha,\Omega,\phi,d,N_r)\sin\alpha\, d\alpha\, d\Omega\, d\phi \quad (3)$$

Substituting eq 1 into eq 3 and accounting for the definition of the zero-order Bessel function, $J_0(qd_{mn}\sin\alpha) = (1/\pi)\int_0^\pi \exp(i\mathbf{qd}_{mn})\,d\phi$, we obtain the following result:

$$\bar{I}_{\text{domain}}(q,L,R,d,N_r) = N_r\bar{I}_1(q,L,R) + \langle I_1(q,L,R,\alpha,\Omega)\sum\sum_{m\neq n}^{N_r} J_0(qd_{mn}\sin\alpha)\rangle_{\alpha,\Omega} \quad (4)$$

This equation generalizes the well-known Debye formula[23] derived for the X-ray scattering from a crystalline powder. But contrary to this case the rod form-factor is dependent on the orientation. Indeed, depending on the analyzer position the functions $I_1(q,L,R,\alpha,\Omega)$ and $\bar{I}_1(q,L,R)$ are given by eqs AI.7 and AI.8 and eqs AI.10 and AI.11, respectively. The angular brackets in eq 4 denote an averaging over the angles α and Ω. The sums in eq 4 are estimated in Appendix II for $N_r = 7$ and 22 under the assumption that the most probable distribution of centers of parallel rods within the domain matches the hexagonal lattice.

The distribution of the shortest distance d between the rods is supposed to represent the log−normal function

$$f(d) = \frac{1}{d\sigma_d\sqrt{2\pi}}\exp\left[-\frac{(\ln d - \ln \bar{d})^2}{2\sigma_d^2}\right] \quad (5)$$

characterized by the average value $\bar{d}$ and its dispersion σ_d. Thus, the light scattering intensity from a set of noncorrelated domains is given by the following integral

$$\langle I_{\text{domain}}(q,L,R,\bar{d},\sigma_d,N_r)\rangle = \int_0^\infty f(d)\bar{I}_{\text{domain}}(q,L,R,d,N_r)\,dd \quad (6)$$

4.3. Light Scattering by Ensemble of Domains. An increase in polymer concentration would lead to an increase in the number of the ordered domains, thus decreasing the distance between them. In turn, this would be expected to result in interference of light scattered by different domains. The relative scattering intensity from the ensemble of N_d domains may be described by the following expression:

$$I_{\text{ensemble}} = \langle I_{\text{domain}}(q,L,R,\bar{d},\sigma_d,N_r)\rangle\left\{1 + \frac{1}{N_d}\sum\sum_{k\neq l}^{N_d}\exp(i\mathbf{qh}_{kl})\right\} \quad (7)$$

where $\mathbf{h}_{kl}$ is the distance between the centers of k-th and l-th domains. Averaging eq 7 over orientations of $\mathbf{h}_{kl}$, we obtain the following result:

$$\bar{I}_{\text{ensemble}}(q,L,R,\bar{d},\sigma_d,\bar{h},N_r,N_d) = \langle I_{\text{domain}}(q,L,R,\bar{d},\sigma_d,N_r)\rangle\left\{1 + \frac{1}{N_d}\sum\sum_{k\neq l}^{N_d}\frac{\sin(qh_{kl})}{qh_{kl}}\right\} \quad (8)$$

This expression is identical to the Debye formula[23] with the exception that a molecular form-factor is replaced by the average scattering intensity of noncorrelated domains.

5. Discussion

A correlation of the structural characteristics of PVDF−acetone solutions with the observed optical properties is discussed in this section. The structural parameters can be defined through comparison of the obtained experimental data with results of theoretical modeling of light scattering from the ordered domains. First, the average optical anisotropy δ of the fiberlike elements of the domains is estimated. This may be done through an evaluation of the ratio of small-angle H_V to V_V scattering intensities, $a = I_{HV}/I_{VV}$. According to our measurements this value varies from 0.005 to 0.001 for the 2% PVDF−acetone solutions (cf. Figures 1 and 2). For definiteness we will consider $a \cong 0.002$. Comparing this ratio with the theoretical one developed from eqs AI.10 and AI.11, we obtain the following equation for the unknown parameter δ:

$$[-3aD_0 + 2(2-a)D_1 + (4-3a)D_2]\delta^2 + 8a[(D_0+D_1)\delta - D_0] = 0 \quad (9)$$

where D_1, D_2, and D_3 are defined by eq AI.12. The second-order term with respect to q is neglected here because of the low value of the concerned scattering angle. A subsequent numerical analysis of eq 9 shows that the optical anisotropy δ is restricted between 0.17 and 0.23 for a broad range of microfiber dimensions, i.e., $L = (1 \div 10)\lambda$ and $R = (0.01 \div 1)\lambda$. This implies that the ratio of the longitudinal to the transversal polarizability of polymer microfibers in the PVDF−acetone solutions should lie in the range 1.2−1.3. The average value $\alpha_\parallel/\alpha_\perp = 1.25$ corresponding to $\delta = 0.2$ will be considered below.

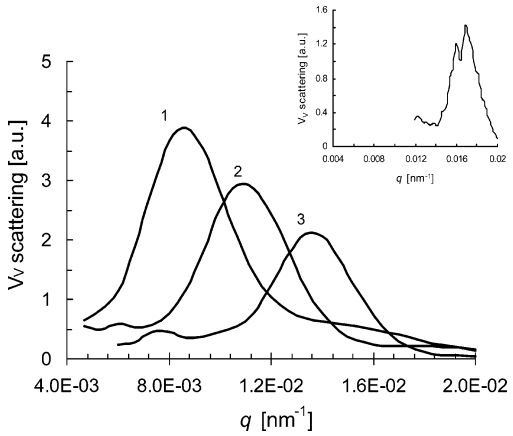

Figure 10. Theoretical V_V scattering profiles for three types of randomly oriented domains composed of $N_r = 22$ rods with $L = 6\lambda$ and $R = 0.3\lambda$: (1) $d = 1.7\lambda$, $\sigma_d = 0.022$ log λ; (2) $d = 1.35\lambda$, $\sigma_d = 0.015$ log λ; (3) $d = 1.1\lambda$, $\sigma_d = 0.01$ log λ. The inset corresponds to the V_V scattering from the ensemble of $N_d = 27$ domains ($\bar{d} = 0.9\lambda$ $\sigma_d = 0.004\lambda$) with $h = 8\lambda$.

As it follows from eq 6, the light scattering intensity by a set of randomly orientated domains of ordered microfibers is dependent on five structural parameters: the longitudinal and transversal sizes, L and $2R$, of the microfibers, the average inter-fiber distance $\bar{d}$, the dispersion σ_d of the distance, and the average number N_r of microfibers per domain. We are going to find correlation of these parameters with angular position and amplitude of the scattering peak.

Theoretical V_V and H_V scattering curves based on the model approximation of the structure of PVDF−acetone solutions are represented in Figures 10 and 11. During this modeling we used an intuitive assumption that an increase in PVDF concentration should be followed by a decrease in dispersion σ_d due to an ordering of the solution structure. This resulted in scattered peaks, which are similar to those observed in the experiments (see Figures 1 and 2). This implies that the proposed model of the scattering domain retains characteristic features of the solution structure being thus appropriate for a quantitative analysis of scattering profiles.

With the exception of the small-angle scattering, limited by the range $q = 0 \div 4 \times 10^{-3}$ nm^{-1}, the observed scattering profiles (Figures 1−4) may be treated as a superposition of the

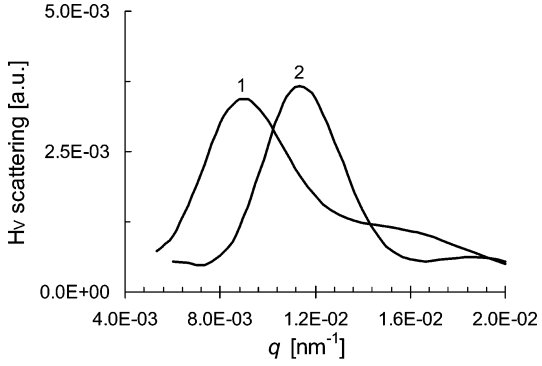

Figure 11. Theoretical H_V scattering profiles for two types of domains composed of $N_r = 22$ rods with $L = 6\lambda$ and $R = 0.3\lambda$: (1) $d = 1.7\lambda$, $\sigma_d = 0.022 \log \lambda$; (2) $d = 1.35\lambda$, $\sigma_d = 0.015 \log \lambda$.

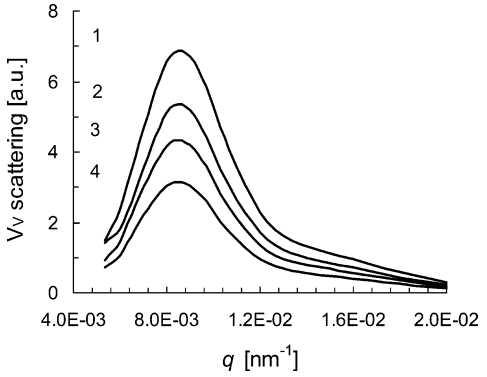

Figure 12. Dependence of theoretical V_V scattering profiles of randomly oriented domains ($N_r = 22$, $R = 0.3\lambda$, $d = 1.7\lambda$, and $\sigma_d = 0.022 \log \lambda$) on the rods length: (1) $L = 3\lambda$; (2) $L = 4\lambda$; (3) $L = 5\lambda$; (4) $L = 7\lambda$.

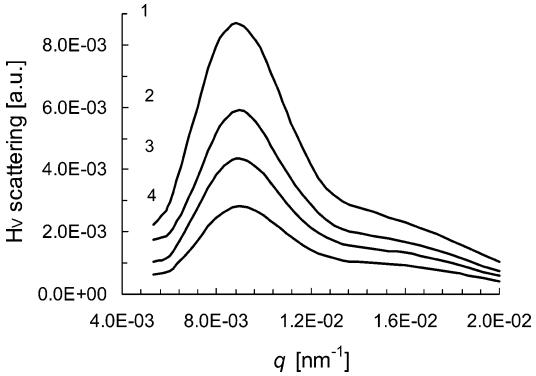

Figure 13. Dependence of theoretical H_V scattering profiles of randomly oriented domains ($N_r = 22$, $R = 0.3\lambda$, $d = 1.7\lambda$, and $\sigma_d = 0.022 \log \lambda$) on the rods length: (1) $L = 3\lambda$; (2) $L = 4\lambda$; (3) $L = 5\lambda$; (4) $L = 7\lambda$.

Bragg peaks contributed by different domains with a fixed average distance between the microfibers. Actually, it is found that an increase in the average number of rods N_r per domain leads to the appearance of high-order peaks accompanied by growing and narrowing of the main peak, which remains in the same position. The numerical analysis shows that variation of rod sizes, L and R, does not influence the position of the main peak as well. On the other hand, a decrease in radii of microfibers results in growing of the secondary peaks. This effect is more pronounced for H_V scattering, which is found to be more sensitive to the transversal size R than V_V scattering. However, if R is large enough, the secondary peaks in the H_V scattering profile become smoother or completely disappear. In the latter case, theoretical V_V scattering curves contain just a single peak that is in agreement with experimental observations (cf. Figures 2 and 4). This regularity could be used to estimate the low boundary of the transversal dimension of polymer microfibers, which is found to match $R \cong 0.3\lambda$. It is worth noting that the obtained value is compatible with the cross-section of polymer ligaments of the PVDF film as it is seen in electron microscopy (Figure 7).

The numerical analysis suggests that the average inter-fiber distance $\bar{d}$ and the length L of microfibers are the most relevant parameters influencing angular position and magnitude of the scattering peak. Figures 10 and 11 demonstrate the role of $\bar{d}$ in V_V and H_V scattering. It is seen that a decrease in the average distance between the neighboring microfibers in domains leads to a shift of the main peak toward the larger scattering vectors. This result is in line with the general diffraction theory. On the other hand, a change in the microfiber length results in significant alteration in magnitude of the scattering peak: the smaller the L, the higher the peak. At the same time, variation of L does not affect the angular position of the peak and does not give rise to secondary peaks (cf. Figures 12 and 13).

A comparison of the experimental V_V and H_V scattering data (Figures 1 and 2) and the corresponding to theoretical profiles (Figures 10 and 11) indicates that the average distance $\bar{d}$ between microfibers correlates with polymer concentration. Indeed, the V_V scattering curves, measured in 2%, 5%, and 10% PVDF−acetone solutions (see Figure 1), can be adequately described within the proposed model if the average inter-fiber distance $\bar{d}$ is equal to 1.7λ, 1.35λ, and 1.1λ respectively. In other words, an increase in polymer concentration leads to reduction of the average inter-fiber distance. Moreover, it is easy to check that the value of the scattering vector q^* corresponding to the position of the maximum peak intensity is a decreasing function of $\bar{d}$. This dependence is in agreement with the previously mentioned behavior of q^* as a function of polymer concentration (see section 3.1 and Figure 5). The above analysis therefore suggests that the structure of the PVDF−acetone solutions studied comprises a close packing of ordered domains of polymer microfibers.

Figures 10 and 11 indicate that the above theoretical model describes equally as well the opposite behavior of the V_V and H_V scattering intensities with variation of average inter-fiber distance i.e., the smaller the value of $\bar{d}$, the smaller the magnitude of V_V, while the larger the H_V peak (cf. Figures 1 and 2). This observation reveals the effect of redistribution of scattering intensity among nonpolarized and depolarized light.

The observed behavior of scattering peaks with temperature shows that the amplitude grows while the angular position remains fixed for both V_V and H_V (see Figures 3 and 4). In addition, there is no evidence of appearance of secondary peaks with increase in temperature. This demonstrates that neither average inter-fiber distance nor transversal sizes of the fibers are sensitive to temperature. Otherwise, the main peak would be shifted and secondary peaks may come into sight. The increase in the peak amplitude with temperature can be explained either by increasing in number N_r of microfibers per scattering domain or by decreasing in average fiber length L. We suppose that the latter assumption is more reasonable. Actually, the elevation of temperature could result in the destruction of physical bonds between neighboring PVDF chains leading to softening of microfibers. In turn, this may give rise to an increase in flexibility of the microfibers, thus shortening the effective fiber length for each domain. This effect is demonstrated in Figures 12 and 13 by the example of V_V and H_V light scattering. On the other hand, an increase in N_r would inevitably be followed by a decrease in the cross-sectional size

of the microfibers leading to the appearance of secondary scattering peaks, which are not the case for PVDF−acetone solutions below the gel point (see Figures 3 and 4).

If the PVDF concentration exceeds 10%, strong modulations of scattering peaks could be observed. An example corresponding to a 20% PVDF−acetone solution is given in the inset of Figure 1. The model of randomly orientated domains discussed above does not explain this type of scattering profile. To clarify this phenomenon, the interference of light scattered by an ensembleof N_d domains has to be taken into account as it is suggested in section 4.3. The corresponding result is depicted in the inset of Figure 10. The obtained scattering profile was calculated from eq 8. For the sake of simplicity, the centers of the domains were arranged in nodes of a simple cubic lattice. The intensity modulations within the peak are clearly observed in the inset. However, the interference of scattered light does not cause a shift in the angular position of the main peak.

Multiple scattering is an additional issue, which should be discussed in this paper. Normally, it contributes to the V_V scattering and affects the accuracy of measured sizes of scattering elements:[24,25] the larger the polymer concentration, the more the influence of multiple scattering. Nevertheless, it is hardly to expect that multiple scattering sways the H_V scattering. The simultaneous observation of similar peaks at V_V and H_V scattering permits to conclude that the studied optical phenomenon is not affected by the multiple scattering and arises due to interference of light scattered by the ordered domains. Moreover, the studied PVDF solutions are transparent showing just a small opalescence within the range of polymer concentration between 1% and 10%. This allows claiming that the multiple scattering does not visibly alter the obtained average dimensions and distance between the microfibers. It is clear that at higher polymer concentration, especially above physical gelation point, the contribution of multiple scattering may embarrass calculation of solution structural parameters. Nevertheless, the proposed approach explains the existence of scattering peak as well as its oscillating nature even for 20% PVDF solutions.

6. Conclusion

The wide-angle light scattering from PVDF−acetone solutions reveals scattering peaks for both V_V and H_V scattering. The angular position of the peak is found to be very sensitive to the concentration of the polymer: the higher the concentration, the larger the scattering angle corresponding to the peak position. An increase in temperature leads to a growth in the amplitude of the scattering peak without shift of the peak position. Comparison of these data with the proposed theoretical model suggests that the morphology of the PVDF−acetone solution may be represented as a close packing of ordered fibrillar domains. It is found that (i) an increase in PVDF concentration results in a decrease in the average distance between the neighboring microfibers and (ii) an increase in temperature causes a decrease in the average length of the microfibers.

The obtained results demonstrate that PVDF−acetone solutions belong to an important class of polymer systems whose morphology is represented by hierarchy of self-organized structures consisting of microfibers grouped into the ordered domains. This type of structures is found to appear at rather low polymer concentration. Several questions follow from our study. What is the physical origin of the observed many-scale hierarchy? What types of polymer solutions could provide similar structural organization? The investigation of these problems seems of high importance.

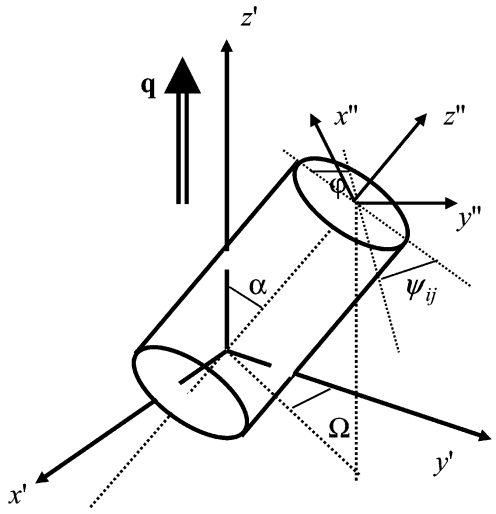

Figure 14. Position of scattering element in the (x', y', z') coordinate frame attached to the scattering vector **q**. (x'', y'', z'') is the local coordinate system of the rod.

Acknowledgment. The authors are grateful to Michel Duval for his help in characterization of PVDF dilute solutions by dynamic light scattering. We thank Bernard Lotz for his assistance with the microscope and TEM studies. S.P. expresses the sincere gratitude for the hospitality during his work at ICS.

Appendix I. Depolarized Light Scattering from a Single Rod

The light scattering intensity from a single rod of arbitrary orientation is given by the following expression:

$$I_1 = (\mathbf{MO})^2\{\int_V \exp[k(\mathbf{rs})]\, d\mathbf{r}\}^2 \qquad \text{(AI.1)}$$

Since our measurements were done in the horizontal (x,y)-plane, the unit vector **s** along the scattering vector is

$$\mathbf{s} = \mathbf{i}\sin\frac{\theta}{2} - \mathbf{j}\cos\frac{\theta}{2} \qquad \text{(AI.2)}$$

The vector **M** denotes the dipole moment induced in a single rod by the incident light with electric field $\mathbf{E}_0 = E_0\mathbf{k}$:

$$\mathbf{M} = \alpha\mathbf{E}_0 = E_0\alpha\mathbf{k} \qquad \text{(AI.3)}$$

α is the polarizability tensor of the rod relative to the solvent. In the case of uniaxial optical anisotropy, this tensor is characterized by the longitudinal $\alpha_{||}$ and transversal $\alpha_\perp$ polarizabilities in its principal coordinate system (see Figure 14). The anisotropy degree of the rod is thus defined as $\delta = 1 - \alpha_\perp/\alpha_{||}$.

The vector **O** of eq AI.1 is a unit vector along the transmission direction of the analyzer.[14] At the vertical position of the analyzer, this vector is given by $\mathbf{O}_V = \mathbf{k}$, while at the horizontal position $\mathbf{O}_H = -\mathbf{i}\sin\theta + \mathbf{j}\cos\theta$ (at $\mu = 90°$). Note that **i**, **j**, and **k** are the basis vectors of the laboratory coordinate system directed along the x-, y-, and z-axes, respectively.

The orientation of the rod axes is conveniently fixed relative the reference framework by associating the axes with the scattering vector **q**. For the z'-axis along **q**, the rod orientation is defined by the polar, α, and azimuth, Ω, angles depicted in Figure 14. In this case the products $\mathbf{MO}_H$ and $\mathbf{MO}_V$ take the following forms:

$$\mathbf{MO}_V = E_0\alpha_{||}(\delta \sin^2\alpha \sin^2\Omega + 1) \quad \text{(AI.4)}$$

$$\mathbf{MO}_H = -E_0\alpha_{||}\delta \sin\alpha \sin\Omega \left(\sin\alpha \cos\Omega \sin\frac{\theta}{2} + \cos\alpha \cos\frac{\theta}{2}\right) \quad \text{(AI.5)}$$

The form factor of the cylindrical rod of length L and radius of cross-section R is[3]

$$F(q,L,R,\alpha) = \int_V \exp[k(\mathbf{rs})]\, d\mathbf{r} = 2V\frac{\sin(qL\cos\alpha/2)}{qL\cos\alpha/2}\frac{J_1(qR\sin\alpha)}{qR\sin\alpha} \quad \text{(AI.6)}$$

$J_n(x)$ is a Bessel function of the nth order. Substituting eqs AI.4−AI.6 into eq AI.1, we obtain V_V and H_V scattering intensities from a single rod at the fixed orientation:

$$I_{1,VV}(q,L,R,\alpha,\Omega) = E_0^2\alpha_{||}^2F^2(q,L,R,\alpha)[\delta \sin^2\alpha \sin^2\Omega + 1]^2 \quad \text{(AI.7)}$$

$$I_{1,HV}(q,L,R,\alpha,\Omega) = E_0^2\alpha_{||}^2F^2(q,L,R,\alpha)\delta^2 \sin^2\alpha \sin^2\Omega \left(\sin\alpha \cos\Omega \sin\frac{\theta}{2} + \cos\alpha \cos\frac{\theta}{2}\right)^2 \quad \text{(AI.8)}$$

Equation AI.1 averaged over all orientations gives the intensity of light scattered by a set of noncorrelated and randomly oriented rods:

$$\bar{I}_1(q,L,R) = \frac{1}{4\pi}\int_0^{\pi}\int_0^{2\pi} I_1(q,L,R,\alpha,\Omega)\sin\alpha\, d\alpha\, d\Omega \quad \text{(AI.9)}$$

Substitution of eqs AI.6−AI.8 into eq AI.9 leads to the following solutions:

$$\bar{I}_{1,VV}(q,L,R) = \frac{1}{8}E_0^2\alpha_{||}^2\{\delta^2(3D_0 + 2D_1 + 3D_2) - 8\delta(D_0 + D_1) + 8D_0\} \quad \text{(AI.10)}$$

$$\bar{I}_{1,HV}(q,L,R) = \frac{1}{8}E_0^2\alpha_{||}^2\delta^2\left\{4(D_1 - D_2) + \sin^2\frac{\theta}{2}[5D_2 - 6D_1 + D_0]\right\} \quad \text{(AI.11)}$$

The values D_n are given by integrals

$$D_n(q,L,R) = 2\int_0^{\pi}\left[\frac{\sin(qL\cos\alpha/2)}{qL\cos\alpha/2}\frac{J_1(qR\sin\alpha)}{qR\sin\alpha}\right]^2\cos^{2n}\alpha\sin\alpha\, d\alpha \quad (n = 0, 1, 2) \quad \text{(AI.12)}$$

which depend on rod sizes and value of the scattering vector.

Appendix II. Evaluation for Sums

To estimate sums $S_{Nr} = \sum\sum_{m\neq n}^{N_r} J_0(qd_{mn}\sin\alpha)$ in eq 4, we assume that the centers of parallel rods are arranged in a hexagonal lattice in a framework of the model under consideration. In the case of domains containing 7 and 22 rods, the following expressions for the sums are obtained:

$$S_7 = 6[4J_0(qd\sin\alpha) + J_0(2qd\sin\alpha) + 2J_0(qd\sqrt{3}\sin\alpha)] \quad \text{(AII.1)}$$

$$S_{22} = 2[49J_0(qd\sin\alpha) + 30J_0(2qd\sin\alpha) + 19J_0(3qd\sin\alpha) + 6J_0(4qd\sin\alpha) + 37J_0(qd\sqrt{3}\sin\alpha) + 16J_0(2qd\sqrt{3}\sin\alpha) + 46J_0(qd\sqrt{7}\sin\alpha) + 22J_0(qd\sqrt{13}\sin\alpha) + 6J_0(qd\sqrt{19}\sin\alpha) + 2J_0(qd\sqrt{21}\sin\alpha)] \quad \text{(AII.2)}$$

Supporting Information Available: Text discussing dynamic light scattering, static light scattering, and the Guinier plot, with a table showing the dependence of D_Z, R_H, and ρ on scattering angles and concentrations, and figures showing the normalized intensity correlation function, solutions for hydrodynamic radii, D vs c at scattering angle 30°, a Berry plot for PVDF−acetone, Guinier plots for four dilute PVDF−acetone solutions, and comparison of $\ln(K_c/I_{VV})$ vs q^2 dependences for PVDF−acetone solutions. This material is available free of charge via the Internet at http://pubs.acs.org.

References and Notes

(1) Cohen, C.; Tanny, G. B.; Prager, S. *J. Polym. Sci., Polym. Phys. Ed.* **1979**, *17*, 477.
(2) Yilmaz, L.; McHugh, A. J. *Appl. Polym. Sci.* **1986**, *31*, 997.
(3) Altena, F. W.; Smolders, C. A. *Macromolecules* **1982**, *15*, 1491.
(4) Cheng, L. P. *Macromolecules* **1999**, *32*, 6668.
(5) Cheng, L. P.; Young, T. H.; Fang, L.; Gau, J. J. *Polymer* **1999**, *40*, 2395.
(6) Lovinger, A. J. In *Developments in semicrystalline polymers*; Bassett, D. C., Ed.; Applied Science Publisher: Oxford, U.K., 1988.
(7) Guenet, J. M. *Trends Polym. Sci.* **1996**, *4*, 6.
(8) Guenet, J. M. *Thermoreversible Gelation of Polymers and Biopolymers*; Academic Press: London, 1992.
(9) Tazaki, M.; Homma, T. *Rep. Prog. Polym. Phys. Jpn.* **1992**, *35*, 99.
(10) Cakmak, M.; Teitge, A.; Zachmann, H. G.; White, J. L. *J. Polym. Sci., Part B: Polym. Phys. Ed.* **1993**, *31*, 371.
(11) Cheung, Y. W.; Stein, R. S.; Lin J. S.; Wignall, G. D. *Macromolecules* **1994**, *27*, 2520.
(12) Picot, C.; Terrisse, J. Private communications, 1998.
(13) Libeyre, A.; Sarazin, D.; François, J. *Polym. Bull. (Berlin)* **1981**, *4*, 53.
(14) Fuller, G. G. *Optical Rheometry of Complex Fluids: Theory and Practice of Optical Rheometry*; Oxford University Press: Oxford, U.K., 1995.
(15) Cais, R. E.; Kometani, J. M. *Macromolecules* **1985**, *18*, 1354.
(16) Lutringer, G.; Meurer, B.; Weill, G. *Polymer* **1991**, *32*, 884.
(17) Flory, P. J. *Principles of polymer chemistry*; Cornell University Press: Ithaca, NY, 1978.
(18) Berne, B. J.; Pecora, R. *Dynamic Light Scattering with Application to Chemistry, Biology and Physics*; Wiley-Interscience: New York, 1976.
(19) Provencher, S. W. *Comput. Phys. Commun.* **1982**, *27*, 229.
(20) Clough, S.; van Aartsen, J. J.; Stein, R. S. *J. Appl. Phys.* **1965**, *36*, 3072.
(21) Pedersen, J. S. *Adv. Colliod Interface Sci.* **1997**, *70*, 171.
(22) Van Aartsen, J. J. *Eur. Polym. J.* **1970**, *6*, 1095.
(23) Guinier, A.; Fournet, A. *Small Angle Scattering of X-rays*; Chapman and Hall Ltd.: New York, 1955.
(24) Berry, G. C. Light scattering, classical: Size and size distribution characterization. In *Encylcopedia of Analytical Chemistry: Instrumentation and Applications*; Meyers, R. A., Ed.; John Wiley & Sons, Ltd.: Sussex, U.K., 2000.
(25) Kokhanovsky, A. A.; Weichert, R. *Appl. Opt.* **2001**, *40*, 1507.

MA050697E